



1 **Effects of long-range transport of air pollutants on nitrogenous organic matters in**
2 **mountain background region of Southeast China: Sources and influencing factors**
3 **identified by observation and modal calculation**

4

5 Yanqin Ren¹, Gehui Wang², Jie Wei³, Jun Tao⁴, Zhisheng Zhang⁴, Hong Li¹

6

7

8

9

10

11 ¹State Key Laboratory of Environmental Criteria and Risk Assessment, Chinese
12 Research Academy of Environmental Sciences, Beijing 100012, China

13 ²Key Lab of Geographic Information Science of Ministry of Education of China,
14 School of Geographic Sciences, East China Normal University, Shanghai 200142,
15 China

16 ³Key Laboratory of Ecosystem Network Observation and Modeling, Institute of
17 Geographic Sciences and Natural Resources Research, Chinese Academy of
18 Sciences, Beijing 100101, China

19 ⁴South China Institute of Environmental Sciences, Ministry of Ecology and
20 Environment, Guangzhou, 510655, China

21

22

23 Correspondence: Gehui Wang (ghwang@geo.ecnu.edu.cn) and Jie Wei
24 (weijie@igsnr.ac.cn)

25

26

27

28

29



30 **Abstract**

31 Nitrated aromatic compounds (NACs), a major component of brown carbon (BrC),
32 have a significant role in the atmosphere's ability to absorb light. Despite this, the
33 sources and major influencing variables of the mountain background atmosphere are
34 mostly lacking. The current work is based on a thorough field investigation of NACs
35 from fine particle samples taken in 2014 and 2015 at the peak of Mt. Wuyi (1139 meters
36 above sea level) and includes a thorough examination of the seasonal fluctuations in
37 their composition, sources, and significant influencing factors. As a result of the air
38 masses traveling mostly via northern heating zones, the total abundance of nine
39 quantifiable NACs increased significantly in the winter ($3.9 \pm 1.5 \text{ ng m}^{-3}$) and autumn
40 ($2.1 \pm 0.94 \text{ ng m}^{-3}$), whereas it decreased in the spring ($1.3 \pm 0.75 \text{ ng m}^{-3}$) and summer
41 ($0.97 \pm 0.36 \text{ ng m}^{-3}$). The most prevalent NAC species during the year was 4-
42 nitrocatechol (25.8%), followed by 5-nitroguaiacol (17.6%). In addition, the majority
43 of NACs (93%) were influenced by coal, biomass, and petroleum combustion over the
44 entire year, according to the results of structural equation modeling (SEM). Pollutant
45 movement had a significant impact on the atmospheric NACs at the peak of Mt. Wuyi,
46 especially in the winter (93.4%) and spring (68.7%). Long-range transport of nitration
47 reactions was the dominant style in the transport process during the winter (33.7%),
48 while long-range transport of mixed sources was significant throughout the other
49 seasons (14%–37%). In particular, for 4-nitrocatechol, NO_2 may enhance the generation
50 of NACs with a major impact on their compositions. Under low- NO_x conditions, the



51 formation of NACs was comparatively sensitive to NO_2 , suggesting that NACs would
52 become significant in the aerosol characteristics when nitrate concentrations decreased
53 as a result of emission reduction measures.

54 **1 Introduction**

55 One of the most important constituents of BrC is nitrated aromatic compounds
56 (NACs), which have an aromatic moiety and the -OH and - NO_2 functions (Desyaterik
57 et al., 2013; Wu et al., 2020). Nitrophenols (NPs), nitrosalicylic acids (NSAs),
58 nitroguaiacols (NGAs), and nitrocatechols (NCs) are the most common among various
59 kinds of NACs. Due to their capacity to absorb light, they have received a lot of
60 attention (Li et al., 2020c; Wang et al., 2018; Teich et al., 2017; Wang et al., 2016), and
61 ~4% of the net water-soluble BrC absorption has been ascribed to them as documented
62 by several earlier studies (Mohr et al., 2013; Zhang et al., 2013). Because of NACs'
63 strong mutagenicity, cytotoxicity, and carcinogenicity, they manifest an influence on
64 human health (Iinuma et al., 2010).

65 Various ambient atmospheres has been shown to have NACs, including rural
66 (Liang et al., 2020; Teich et al., 2017; Lv et al., 2022), urban (Li et al., 2020b; Li et al.,
67 2020c; Wang et al., 2019; Ren et al., 2022; Li et al., 2020a), suburban (Kitanovski et
68 al., 2021), and mountain (Wang et al., 2018). They can not only originate from primary
69 emissions, but also can be created *in-situ* by secondary formation. Biomass burning
70 (Wang et al., 2017; Lin et al., 2017; Chow et al., 2015), traffic emissions (Lu et al.,
71 2019a), and coal combustions (Lu et al., 2019b) are the key primary sources of NACs.



72 Several works indicated that the primary cause of the generation of NACs is biomass
73 burning (Lin et al., 2017; Wang et al., 2017; Mohr et al., 2013), whereas several other
74 studies consider road traffic emissions as the primary cause of the origin of nitrophenols
75 (Zhang et al., 2010). Secondary chemistry primarily classified as the nitration of
76 aromatic compounds, may occur in both aqueous and gas phases (Li et al., 2020c;
77 Harrison et al., 2005; Wang et al., 2019). According to recent research, phenolic VOCs
78 being oxidized by the nitrate radical ($\text{NO}_3\bullet$) at night may also function as a notable
79 source of nitrophenols and additional BrC species (Mayorga et al., 2021). Even though
80 researchers have started to study NACs, very little is known regarding the relative
81 significance of their corresponding primary and secondary sources. The fundamental
82 variables affecting the generation of NACs are also little known because only a few
83 investigations have been conducted thus far, in particular within China.

84 Field observations in both clean and polluted environments are essential for better
85 identifying elements that have previously gone unnoticed and for confirming the
86 mechanistic understanding attained from research on smog chambers. These studies are
87 nonetheless concerning, particularly those carried out in environments with low
88 concentrations of anthropogenic pollutants like NO_x . In our earlier research, we
89 examined how biomass burning affects biogenic secondary organic aerosol (BSOA)
90 production from long-haul travel and how biogenic volatile organic compounds
91 (BVOCs) contribute to the generation of BSOA in high mountain locations (Mt. Wuyi).
92 Nine NACs (NPs, NGAs, NCs, and NSAs) in the $\text{PM}_{2.5}$ were studied in the current
93 study, to better understand ambient characteristics of NACs, their chief primary sources,



94 and the principal factors influencing their secondary development, particularly the
95 effect of long-range transport of air pollutants. PM_{2.5} samples that were collected over
96 an entire year on Mt. Wuyi's summit were measured using GC-MS. The outcome of the
97 current research offers useful insight into the information characteristics of NACs via
98 seasonal variation in sources, and they can provide insightful information about the
99 potential influences on the second generation of NACs in background environments
100 that are relatively free of contaminants.

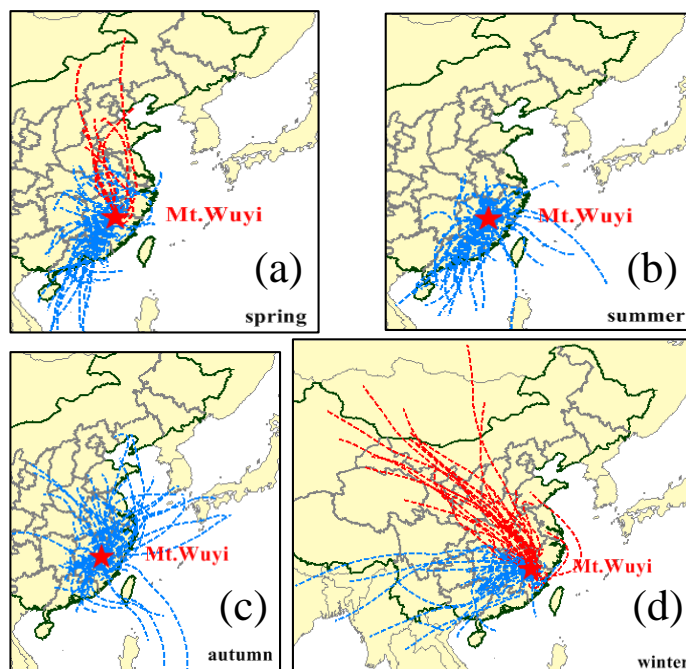
101 **2 Experimental**

102 **2.1 Sample site and field observations**

103 One national atmospheric background monitoring station is located at Mt. Wuyi
104 station (27°35'N, 117°43'E, 1139 m a.s.l., Fig. 1). There are no evident sources of
105 atmospheric pollution within 50 km² of the monitoring station, which is located at the
106 southern tip of the Mt. Wuyi national reserve. As a result, it can accurately depict the
107 atmospheric background conditions of southeast China's forest and mountain region.
108 Due to its high altitude and active airstream, it can also be used to observe the effects
109 of long-range transport. In this work, we used a high-volume air sampler (TE-6070V,
110 Tisch Inc., USA) to gather PM_{2.5} samples with an airflow equivalent to 1.063 m³ min⁻¹.
111 49 PM_{2.5} samples in total were taken over seven days. During the sampling, four
112 blank specimens (one for individual seasons) were obtained. At the same time, we
113 gathered data on conventional pollutants and weather-related pollutants, including
114 temperature (T), relative humidity (RH), SO₂, NO₂, and O₃. Sample site and sampling



115 information has been reported in detail in the literature (Ren et al., 2019).
116



117
118 Fig. 1 Location of the sampling site (Mt. Wuyi: 27°35' N, 117°43' E; 1139 m a.s.l.)
119 and 48 hour backward trajectories reaching the summit during the sampling (spring:
120 March 20, 2014- June 4, 2014; summer: June 4, 2014- September 2, 2014; autumn:
121 September 2, 2014-December 4, 2014; winter: December 4, 2014- February 25,
122 2015).

123 2.2 Chemical analysis

124 Organic compounds, for instance, nine NACs (including 3-methyl-4-nitrophenol
125 (3M4NP), 4-nitrophenol (4NP), 2,4-dinitrophenol (2, 4-DNP), 4-nitroguaiacol (4NGA),
126 5-nitroguaiacol (5NGA), 4-nitrocatechol (4NC), 4-methyl-5-nitrocatechol (4M5NC),
127 3-nitro-salicylic acid (3NSA), 5-nitro-salicylic acid (5NSA)), fossil fuel *n*-alkanes (ff
128 *n*-alkanes), PAHs, trehalose, and levoglucosan were identified in the samples.
129 Elemental carbon (EC), organic carbon (OC) and some inorganic ions (i.e. SO_4^{2-} , NO_3^- ,



130 NH_4^+ , K^+) were also the constituents of the samples. The procedures for sample
131 extraction and derivatization have been elaborated elsewhere (Ren et al., 2022; Ren et
132 al., 2019). Briefly stated, an aliquot of the filter was extracted with a mixture of
133 methanol and dichloromethane (DCM, 1:2) under ultrasonication for three times. The
134 extracts are concentrated and dried by using pure nitrogen, derivatized with N, O-bis-
135 (trimethylsilyl) trifluoroacetamide (BSTFA), and analyzed by using gas
136 chromatography equipped with mass spectroscopy (GC-MS, 7890A/5975C, Agilent
137 Co., USA). The GC separation was carried out on a DB-5MS fused silica capillary
138 column, and the GC oven temperature programmed from 50°C (2min) to 120°C with
139 15°C min⁻¹ and then to 300°C with 5°C min⁻¹, with a final isothermal hold at 300°C for
140 16 min. The sample was injected in a splitless mode at an injector temperature of 280°C,
141 and scanned from 50 to 650 Daltons using electron impact (EI) mode at 70eV. Under
142 the Interagency Monitoring of Protected Visual Environments (IMPROVE)
143 thermal/optical reflectance (TOR) methodology, OC and EC were measured by a DRI
144 model 2001 Carbon Analyze (Atmoslytic Inc., Calabasas, CA, USA). OC collected by
145 filter membrane are first volatilized with the proceeding of temperature up to 580 °C in
146 the protection of He and determined. EC are analyzed then with the increasing of
147 temperature to 840°C in the presence of He and O₂ by the NDIR non-dispersive infrared
148 CO₂ detector. Dionex-600 ion chromatography was used to quantify inorganic ions in
149 samples after extracted with Mili-Q pure water (Thermo Fisher Scientific Inc., USA).



150 **2.3 Model calculation**

151 As a receptor model, Positive Matrix Factorization (PMF) (EPA PMF 5.0 version)
152 has been extensively employed for the source distribution of atmospheric pollutants
153 (Ren et al., 2022; Wu et al., 2020; Wang et al., 2018). To quantify the source
154 apportionment for NACs including transport and local, the mass concentrations of SO₂,
155 NO₂, CO, O₃, sulfate, nitrate, NH₄⁺, K⁺, ff-*n*-alkanes, PAHs, levoglucosan, trehalose
156 3M4NP, 4NP, 4NGA, 5NGA, 2,4-DNP, 4M5NC, 4NC, 5NSA, and 3NSA, were
157 employed as input data. *Q* value and *r*, which were defined as the agreement between
158 the model fit and the correlation between estimated and measured concentrations,
159 respectively, are used to determine the appropriate factor number for modeling (Comero
160 et al., 2009). In the current work, the model was iterated upon using a variety of
161 combinations of the concentration data set and three to six covariates. The best solution
162 was determined to be five components based on the *Q* value and *r*² (Table S1) values.

163 The direct and indirect effects of air pollutants variables on NACs were quantified
164 by utilizing Structural equation modeling (SEM). Initially, a conceptual model of
165 hypothetical linkages was developed using past and theoretical information. The
166 measured data were then integrated into the model using the maximum-likelihood
167 estimation technique. We identified the model that best fits the data by methodically
168 deleting non-significant routes from the base model. The *p*-value, χ^2 -test, goodness-of-
169 fit index (GFI) and root mean square error of approximation (RMSEI) index were used
170 to assess the model's suitability. The conceptual model was acceptable if the *p*-value >
171 0.05, Low RMSEA (<0.08), high GFI (>0.9), and low χ^2 values were regarded as



172 positive model fits. AMOS 24.0 (IBM, Chicago, IL, USA) was used to analyze the
173 above statistical analyses.

174 **2.4 Quality assurance and quality control (QA/QC)**

175 All glassware used were rinsed and baked at 450°C for 8 h and further cleaned by
176 using methanol, DCM and hexane immediately before using. Field blank sample
177 analysis showed no serious contamination (less than 5% of real samples). GC/MS
178 response factors of all organic species were used those of the authentic standards. The
179 recovery experiment was done by spiking the standard solution onto blank filters (n=3)
180 and analyzed using the above procedure. Recoveries of the quantified organic
181 compounds were generally between 80% and 110%. Data reported here were all
182 corrected for the blanks.

183 **3 Results and discussion**

184 **3.1 Meteorological Features and Air masses**

185 From March 2013 through February 2015, a total of four seasons were covered by
186 the sampling campaign. In the area under investigation, the four seasons are typically
187 referred to as spring (March through May), summer (June through August), autumn
188 (September through November), and winter (December through February). The rise in
189 temperatures starts in March, and peaks in July (25 °C), before falling to a minimal
190 value of 2.9 °C in January–February. When determining the origin of air masses at a
191 certain location, air mass backward trajectories are taken into account. The Hybrid



192 Single-Particle Lagrangian Integrated Trajectories (HY-SPLIT) model supplied 48-
193 hour air mass backward trajectories for this study. Although prior research has shown
194 that atmospheric aerosols could potentially not follow the results trajectories due to
195 gravitational settling and scavenging processes (Chen and Siefert, 2004), the air mass
196 backward trajectories furnish important background information on airstreams as well
197 as the plausible origins of the air mass that has been sampled (Chen and Chen, 2008).
198 The source regions of primary aerosol gathered from an area located at a distance from
199 the source location, have been also identified using air mass backward trajectories
200 (Chiapello et al., 1997; Wang et al., 2013; Wang et al., 2014). The 48-hour backward
201 trajectories (Fig. 1) show that during the sample, winds from the north were reaching
202 the top, particularly in winter (Fig. 1d), when there were large concentrations of air
203 pollutants due to anthropogenic emissions. Our prior research has shown that these
204 anthropogenic pollutants considerably increased the generation of biogenic secondary
205 organic aerosols (BSOA) (Ren et al., 2019). This explains why some anthropogenic
206 pollutants, such as SO₂, NO₂, ff-*n*-alkanes (fossil fuel markers), PAHs (coal and fossil
207 fuel markers), levoglucosan (biomass burning markers), SO₄²⁻, NO₃⁻, and others were
208 typically higher in winter or autumn (Table 1).

209

210

211

212

213



Table 1. Concentrations (ng m^{-3}) of organic compounds in $\text{PM}_{2.5}$ samples in Mt. Wuyi during the sampling time.

	spring (n=11)	summer (n=13)	autumn (n=13)	winter (n=12)
$\text{PM}_{2.5}$ ($\mu\text{g m}^{-3}$)	16±5.5 (7.6-24)	14±7.8 (4.9-32)	20±7 (8.3-31)	21±7.8 (5-32)
T ($^{\circ}\text{C}$)	16±3.6 (8.2-21)	23±1.3 (21-25)	17±4.7 (9.6-23)	6.4±2.8 (2.9-11)
RH (%)	78±9.7 (57-89)	79±6.5 (67-91)	75±9.2 (60-92)	64±16 (43-96)
SO_2 ($\mu\text{g m}^{-3}$)	1.7±1.2 (0.5-4)	0.9±0.74 (0.21-2.8)	3.1±2 (0.58-6.5)	6.7±3.9 (0.42-14)
NO_2 ($\mu\text{g m}^{-3}$)	4.2±2.1 (1.8-9.1)	1.7±1.3 (0.31-4.5)	4±1.9 (1.1-8.2)	6.2±2.3 (1.5-10)
CO (mg m^{-3})	0.42±0.07 (0.31-0.55)	0.27±0.08 (0.18-0.45)	0.43±0.09 (0.27-0.58)	0.46±0.07 (0.36-0.58)
O_3 ($\mu\text{g m}^{-3}$)	104±12 (89-121)	82±25 (62-142)	93±20 (68-127)	83±20 (34-109)
OC ($\mu\text{g m}^{-3}$)	2.2±1.2 (0.98-4.7)	1.6±0.86 (0.49-3.7)	3.1±1.5 (0.84-6.1)	4.6±1.9 (0.91-7.3)
EC ($\mu\text{g m}^{-3}$)	0.51±0.11 (0.35-0.68)	0.48±0.20 (0.15-0.83)	0.56±0.15 (0.29-0.78)	0.69±0.13 (0.43-0.89)
Inorganic components (ng m^{-3})				
SO_4^{2-}	6.2±2.2 (2.6-9.8)	5.0±3.9 (1.2-15)	7.6±2.9 (2.8-11)	6.3±3.0 (1.1-13)
NO_3^-	0.06±0.11 (NA ^a -0.39)	0.01±0.02 (0.002-0.06)	0.19±0.39 (0.008-1.5)	1.3±1.1 (0.07-4.2)
NH_4^+	1.7±0.55 (0.75-2.3)	1.4±1.2 (0.3-4.5)	2.3±0.99 (0.72-3.8)	2.2±1.2 (0.36-5.1)
K^+	0.21±0.1 (0.08-0.42)	0.13±0.14 (0.03-0.46)	0.28±0.15 (0.06-0.49)	0.39±0.15 (0.08-0.59)
Nitrated aromatic compounds (ng m^{-3})				
4-nitrophenol (4NP)	0.18±0.13 (0.04-0.49)	0.05±0.04 (0.01-0.16)	0.32±0.28 (0.04-1.1)	0.74±0.34 (0.14-1.3)
3-methyl-4-nitrophenol (3M4NP)	0.03±0.03 (0.01-0.09)	0.05±0.02 (0.03-0.08)	0.04±0.02 (0.02-0.09)	0.06±0.04 (0.01-0.12)
2,4-dinitrophenol (2,4- DNP)	0.06±0.03 (0.03-0.13)	0.06±0.03 (0.03-0.14)	0.08±0.03 (0.03-0.14)	0.09±0.05 (0.03-0.18)
4-nitroguaiacol (4NGA)	0.07±0.03 (0.03-0.10)	0.07±0.03 (0.03-0.14)	0.07±0.03 (0.02-0.14)	0.05±0.02 (0.03-0.09)
5-nitroguaiacol (5NGA)	0.21±0.10 (0.06-0.37)	0.29±0.13 (0.07-0.48)	0.32±0.11 (0.11-0.51)	0.22±0.1 (0.07-0.42)
4-nitrocatechol (4NC)	0.34±0.31 (0.07-1.1)	0.14±0.07 (0.03-0.27)	0.64±0.48 (0.13-1.7)	1.6±0.87 (0.27-3.0)



4-methyl-5-nitrocatechol (4M5NC)	0.20±0.08 (0.09-0.33)	0.19±0.06 (0.11-0.31)	0.34±0.1 (0.2-0.53)	0.39±0.19 (0.1-0.73)
3-nitrosalicylic acid (3NSA)	0.07±0.05 (0.03-0.2)	0.04±0.02 (0.01-0.08)	0.09±0.04 (0.04-0.18)	0.19±0.08 (0.04-0.31)
3-nitrosalicylic acid (5NSA)	0.12±0.10 (0.04-0.39)	0.07±0.04 (0.02-0.17)	0.23±0.13 (0.08-0.53)	0.55±0.29 (0.08-1.1)
NACs	1.3±0.75 (0.52-3.1)	0.97±0.36 (0.34-1.7)	2.1±0.94 (0.72-4.0)	3.9±1.5 (1.3-6.3)
Other organic components (ng m⁻³)				
Fossil fuel <i>n</i> -alkanes (ff- <i>n</i> -alkanes)	6.3±3.1 (2.7-12)	3.2±1.3 (1.5-6.1)	9.3±4.7 (3.9-20)	18±5.6 (5.7-28)
PAHs	1.5±0.86 (0.59-3.1)	0.54±0.30 (0.23-1.3)	2.1±1.1 (0.68-4.2)	4.5±1.8 (1.2-6.5)
Levogluconan	15±17 (3.8-62)	4.2±1.7 (1.3-7.5)	23±13 (5.7-41)	52±21 (20-86)
Trehalose	0.63±0.25 (0.29-1.1)	0.87±0.41 (0.25-1.5)	0.49±0.33 (0.23-1.3)	0.36±0.14 (0.12-0.65)

^a NA: not available.

214 3.2 Abundance and seasonal variations of NACs

215 Table 1 lists the measured concentrations of the major PM_{2.5} constituents, and
216 Fig.2 shows the seasonal fluctuations of the nine NACs throughout the year. Nine
217 different NACs' average concentrations varied significantly throughout the year, with
218 winter having the greatest levels (3.9± 1.5 ng m⁻³), followed by autumn (2.1± 0.94 ng
219 m⁻³), spring (1.3± 0.75 ng m⁻³), and summer (0.97± 0.36 ng m⁻³). The total NACs
220 concentrations in the current and earlier works have been compared in Table 2. The
221 total NACs concentration in this study was significantly lower in comparison to that
222 predicted for urban sites in China, particularly in winter and autumn, such as in Beijing
223 (20± 12 ng m⁻³ in autumn, 74± 51 ng m⁻³ in winter) (Li et al., 2020c), Jinan (9.8± 4.2
224 ng m⁻³ in autumn, 48± 26 ng m⁻³ in winter) (Wang et al., 2018), Xi'an (17± 12 ng m⁻³
225 in winter) (Wu et al., 2020), and Hong Kong (12± 14 ng m⁻³ in winter) (Chow et al.,



226 2015). Moreover, as compared to the levels in rural and background sites during
 227 summertime in China, the levels in this work were also much lower, for instance,
 228 Wangdu (Wang et al., 2018), Yucheng, (Wang et al., 2018), Mt.Tai (Wang et al., 2018),
 229 and Xianghe (Teich et al., 2017). In comparison with the studies abroad, the total NAC
 230 concentrations in this investigation were also comparatively lower than the
 231 measurements in winter, such as in the UK (Mohr et al., 2013), Germany (Teich et al.,
 232 2017), Slovenia (Kitanovski et al., 2012) and Belgium (Kahnt et al., 2013).
 233

Table 2. Measured concentrations of nitrated aromatic compounds in domestic and foreign researches over the last decade.

Sampling site	Sampling period	Aerosol Type	NAC Species ^a	Concentrations (ng m ⁻³)	References
Mt. Wuyi, China	Spring, 2014	PM _{2.5}	①②③④⑤ ⑥⑦⑧⑨	1.3 ± 0.75	This study
	Summer, 2014			0.97 ± 0.36	
	Autumn, 2014			2.1 ± 0.94	
	Winter, 2014-2015			3.9 ± 1.5	
Beijing, China	Apr., 2017	PM _{2.5}	①②③④⑤ ⑥⑦⑧⑨	8.6 ± 6.7	Ren et al., 2022
	Jul., 2017			8.5 ± 3.9	
Beijing, China	Sep.-Nov., 2017	PM _{2.5}	①②③④⑥ ⑦⑧⑨	20 ± 12	Li et al., 2020
	Dec., 2017-Feb., 2018			74 ± 51	
Beijing, China	May-Jun., 2016	PM _{2.5}	①②⑥⑦⑩ ⑪⑫⑬	6.6	Wang et al., 2019
Xi'an, China	Jan., 2017	PM _{2.5}	①②③④⑤ ⑥⑦⑧⑨	17 ± 12	Wu et al., 2020
	Jul.-Aug., 2017			0.40 ± 0.27	
Jinan, China	Nov. 2013-Jan., 2014			48 ± 26	
Yucheng, China	Sep., 2014			9.8 ± 4.2	
Wangdu, China	Jun., 2014	PM _{2.5}	①②⑥⑦⑧ ⑨⑩⑪⑫	5.7 ± 2.8	Wang et al., 2018
Wangdu, China	Jun., 2014			5.9 ± 3.8	
Mt.Tai, China	Jul.-Aug., 2014			2.5 ± 1.6	
Wangdu, China	Jun., 2014	PM ₁₀	①②③⑧⑨ ⑩⑬⑭	9.2	Teich et al., 2017
Xianghe, China	Jul.-Aug., 2013			3.6	
Hong Kong, China	Spring, 2010-2012	PM _{2.5}	①②⑥⑦⑩ ⑪⑫⑬	2.7 ± 3.6	Chow et al., 2015
	Summer, 2010-2012			2.2 ± 4.9	
	Autumn, 2010-2012			6.5 ± 6.9	
TROPOS,	Winter, 2009-2012			12 ± 14	
TROPOS,	Jan.-Feb., 2014	PM ₁₀	①②②③⑧	16	Teich et al.,



Germany			⑨⑩⑬⑭		2017
Melpitz,	Jan.-Feb., 2014			12	
Germany	Jul., 2014			0.3	
Waldstein,	Jul., 2014		⑧⑨	0.4	
Germany					
Detling, UK	Jan.-Feb., 2012	PM ₁	①③⑥⑦⑮	19	Mohr et al., 2013
	Spring, 2010			3.8	
Hamme,	Summer, 2010		①⑥⑦	2.2	Kahnt et al., 2013
Flanders,	Autumn, 2010	PM ₁₀	⑪⑫⑬	13	
Belgium	Winter, 2010			32	
Ljubljana,	Dec., 2010-Jan., 2011		①②③④⑤	150	Kitanovski et al., 2012
Slovenia	Aug., 2010	PM ₁₀	⑥⑦⑧⑨⑩ ⑪⑫	0.9	

^a ①4-nitrophenol ②3-methyl-4-nitrophenol ③2,4-dinitrophenol ④4-nitroguaiacol ⑤5-nitroguaiacol
 ⑥4-nitrocatechol ⑦4-methyl-5-nitrocatechol ⑧3-nitro-salicylic acid ⑨5-nitro-salicylic acid ⑩2-
 methyl-4-nitrophenol ⑪3-methyl-5-nitrocatechol ⑫3-methyl-6-nitrocatechol ⑬2,6-dimethyl-4-
 nitrophenol ⑭3,4-dinitrophenol ⑮4-methyl-2-nitrophenol

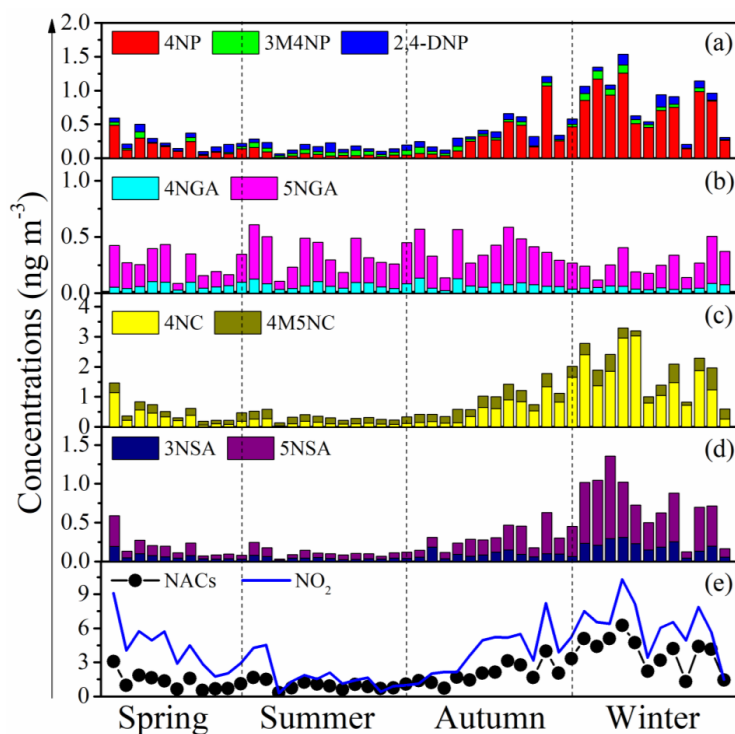
234

235 For each NAC species, NPs (including 4NP, 3M4NP, 2, 4-DNP) (Fig. 2a), NCs
 236 (4NC, 4M5NC included) (Fig. 2c), and NSAs (including 3NSA, 5NSA) (Fig. 2d) have
 237 the same seasonal trends as the total NACs. However, on the contrary, there were no
 238 obvious seasonal trends for NGAs (including 4NAG and 5NGA) (Fig. 2b). 4NC was
 239 on average, the most abundant species throughout the year (25.8%), followed by 5NGA
 240 (17.6%) (Fig. S1), with different proportions of molecular composition in different
 241 seasons (Fig. 3). 4NC was the only NACs species that accounted for more than 20% in
 242 spring (23.7%), autumn (27%), and winter (39.7%). The most prevalent compound over
 243 the summer was 5NGA (28.7%), followed by 4M5NC (20.9%). These findings
 244 contrasted with those of earlier studies on urban areas, which often revealed that 4NP
 245 had the greatest levels, followed by 4NC (Li et al., 2020c; Wang et al., 2018; Wang et
 246 al., 2019). These variations can be due to the various sources and NAC generation



247 processes found in various situations.

248



249

250

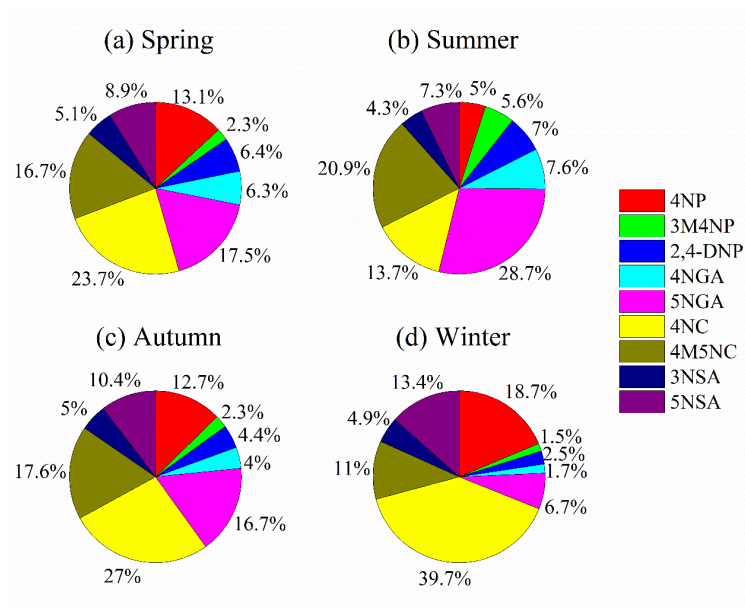
251

252

253

254

Fig.2 Temporal variations of each NACs species (4NP: 4-nitrophenol; 3M4NP: 3-methyl-4-nitrophenol; 2,4-DNP: 2,4-dinitrophenol; 4NGA: 4-nitroguaiacol; 5NGA: 5-nitroguaiacol; 4NC: 4-nitrocatechol; 4M5NC: 4-methyl-5-nitrocatechol; 3NSA: 3-nitrosalicylic acid; 5NSA: 5-nitrosalicylic acid).



255

256 Fig.3 Relative contribution of each NACs species during the sampling time (4NP: 4-
257 nitrophenol; 3M4NP: 3-methyl-4-nitrophenol; 2,4-DNP: 2,4-dinitrophenol; 4NGA: 4-
258 nitroguaiacol; 5NGA: 5-nitroguaiacol; 4NC: 4-nitrocatechol; 4M5NC: 4-methyl-5-
259 nitrocatechol; 3NSA: 3-nitrosalicylic acid; 5NSA: 5-nitrosalicylic acid).

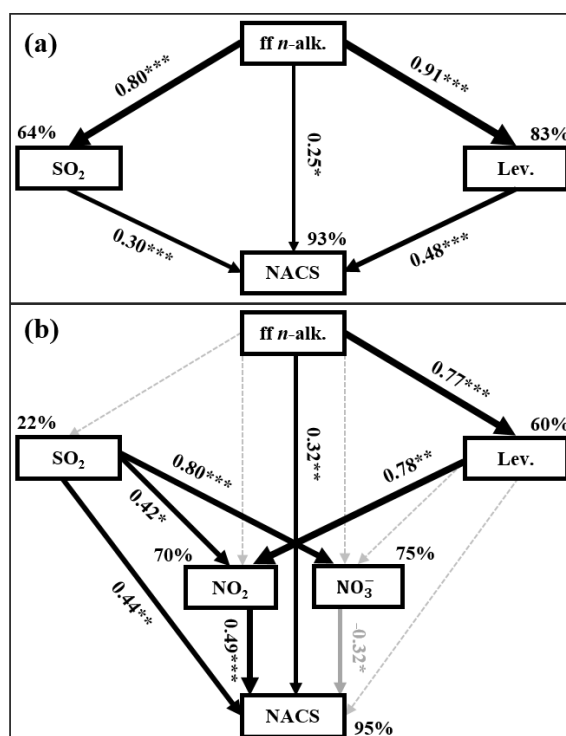
260

261 3.3 Influence factors and sources of NACs

262 For further clarification regarding the influencing factors and sources of NACs,
263 the interrelation between total and individual NAC species and the related pollutants
264 were analyzed based on the results of Pearson correlations depicted in Table 3 (for the
265 whole campaign) and Tables S3-6 (for the four seasons), including PM_{2.5}, SO₂, NO₂,
266 O₃, and other chemical components. It is noteworthy that total NACs and all identified
267 NACs species manifested strong correlations with PM_{2.5} in the whole year, indicating
268 that they are important components of PM_{2.5}. There were good relationships between
269 NACs and primary pollutants in the whole year, such as SO₂ ($r=0.859$, $p<0.01$), ff-*n*-



270 alkanes ($r=0.927$, $p<0.01$), PAHs ($r=0.927$, $p<0.01$), levoglucosan ($r=0.931$, $p<0.01$),
 271 and K^+ (i.e., a BB tracer, $r=0.817$, $p<0.01$) (Table 3). Furthermore, the model calculation
 272 results of SEM indicate ff-*n*-alkanes, SO_2 , and levoglucosan would account for 93% of
 273 NACs (Fig. 4a). All of these connections indicated that burning emissions throughout
 274 the year, such as the burning of coal (Lu et al., 2019b), biomass (Wang et al., 2017; Lin
 275 et al., 2017; Chow et al., 2015), and burning of petroleum (Lu et al., 2019a), had a
 276 substantial impact on NACs.



277
 278 Fig. 4 Structural equation model (SEM) demonstrating the effects of ff *n*-alk., SO_2 , Lev.
 279 and NO_2 on annual (a) or winter (b) mean NACs. The model fits the data well (χ^2
 280 =0.235, $df=1$, $p=0.628$, GFI=0.999, RMSEA=0.000 (a), χ^2 =0.690, $df=2$, p
 281 =0.708, GFI=0.980, RMSEA=0.000 (b)). Black solid arrows indicate significant
 282 positive relationships, gray solid arrows indicate significant negative
 283 relationships and black dashed arrows indicate nonsignificant path coefficients.
 284 The width of arrows is proportional to the strength of path coefficients. Numbers
 285 on arrows are standardized path coefficients (equivalent to correlation



286 coefficients), asterisks following the numbers imply significant relationships (* p
287 < 0.05 , ** $p < 0.01$, *** $p < 0.001$). Percentages (R^2) close to endogenous
288 variables indicate the variance explained by the ff n -alk., SO_2 , Lev. and NO_2 .

289
290 Additionally, total NACs also showed strong correlations with NO_2 ($r=0.862$,
291 $p<0.01$), SO_4^{2-} ($r=0.396$, $p<0.01$), NO_3^- ($r=0.757$, $p<0.01$), NH_4^+ ($r=0.524$, $p<0.01$),
292 probably suggesting that the secondary formation of NACs was also important in the
293 campaign. Here, the NACs concentration was strongly associated with NO_2 , especially
294 in the winter (Fig. 2e), and correlated better than other secondary tracers (Table 3),
295 suggesting that NO_2 is a relatively importance component in the creation of NACs.
296 According to earlier research, the photochemical production of NACs is related to the
297 oxidation of aromatics in the presence of NO_2 , including the $\bullet\text{OH}$ oxidation and the
298 $\text{NO}_3\bullet$ oxidation (Cai et al., 2022; Ren et al., 2022; Yi Chen et al., 2022; Finewax et al.,
299 2018).



Table 3. Pearson correlations between individual NAC species and meteorological parameters, aerosol components, and gas pollutants during the whole campaign (n = 49).

	NACs	4NP	3M4NP	2,4-DNP	4NGA	5NGA	4NC	4M5NC	3NSA	5NSA
PM _{2.5}	0.657**	0.649**	0.376**	0.359*	0.308*	0.521**	0.501**	0.703**	0.561**	0.564**
SO ₂	0.859**	0.887**	0.520**	0.299*	-0.184	-0.053	0.781**	0.637**	0.748**	0.889**
NO ₂	0.862**	0.834**	0.329*	0.347*	-0.142	0.103	0.845**	0.543**	0.762**	0.774**
O ₃	0.146	0.145	0.028	0.024	0.308*	0.403**	0.029	0.348*	0.174	0.102
ff- <i>n</i> -alkanes	0.927**	0.942**	0.364*	0.475**	-0.140	0.090	0.841**	0.732**	0.834**	0.880**
PAHs	0.927**	0.944**	0.486**	0.347*	-0.205	-0.049	0.857**	0.661**	0.838**	0.942**
Levoglucosan	0.931**	0.885**	0.299*	0.392**	-0.207	0.113	0.884**	0.721**	0.881**	0.860**
K ⁺	0.817**	0.805**	0.308*	0.363*	0.109	0.330*	0.707**	0.736**	0.709**	0.732**
SO ₄ ²⁻	0.396**	0.412**	0.281	0.285*	0.411**	0.516**	0.250	0.502**	0.272	0.305*
NO ₃ ⁻	0.757**	0.829**	0.448**	0.322*	-0.225	-0.108	0.701**	0.486**	0.618**	0.766**
NH ₄ ⁺	0.524**	0.560**	0.314*	0.321*	0.276	0.443**	0.385**	0.547**	0.373**	0.442**

**Significant correlation at the 0.01 level.

*Significant correlation at the 0.05 level.

300 Based on the results of the PMF model, this work identified five styles of sources
301 during the campaign to further qualitatively and quantitatively the effects of
302 transportation and local sources of various pollutants emissions on NACs at the summit
303 of Mt. Wuyi. These sources have been shown in Fig. 5 and Fig. 6. As the first source
304 factor, levoglucosan loading was larger in this component profile than it was in other
305 factor profiles due to the long-range transport of biomass burning, also with other high
306 loading anthropogenic primary organic markers, included ff-*n*-alkanes, PAHs, SO₂, and
307 NO₂ (Fig. 5a). Since there was no obvious anthropogenic source at the summit of Mt.
308 Wuyi, this source was assumed to originate from the transmission process. Long-range

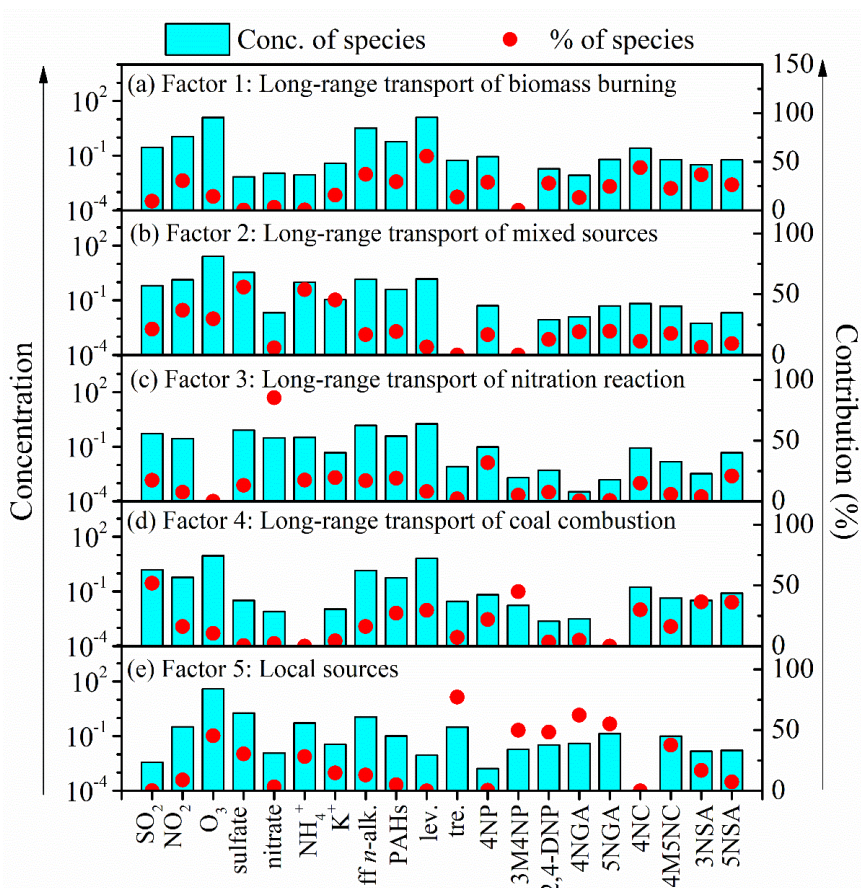


309 transport of mixed sources, with the highest loading of SO₂, NO₂ and K⁺, as well as
310 anthropogenic primary organic markers, was identified as the second source factor
311 during the transmission process, including primary and secondary emissions (Fig. 5b).
312 The third source factor namely long-range transport of nitration reaction showed high
313 concentrations of NO₃⁻ (Fig. 5c). Long-range transport of coal combustion was
314 identified the fourth source factor, with high levels of SO₂ (Fig. 5d). Local sources were
315 recognized as the last source factor, with relatively high levels of O₃ and low levels of
316 anthropogenic pollutants (e.g. SO₂, NO₂, *ff-n*-alkanes, PAHs, levoglucosan) (Fig. 5e).
317 It is noteworthy that trehalose also showed relatively high levels because this
318 component is a naturally existing carbohydrate in vegetations, which were abundant in
319 the sampling site.

320 For the whole campaign year, atmospheric NACs at the summit of Mt. Wuyi was
321 substantially affected by the transport of air pollutants (67%), including long-range
322 transport of mixed sources (21.9%), biomass burning (18.3%), coal combustion (16.5%)
323 and nitration reaction (10.3%). While the impact of local sources accounted for only
324 33% (Fig.5a). The influence of local sources on NACs mainly took place in summer
325 (Fig. 7c), while the other seasons were mainly influenced by the transport of air
326 pollutants (Fig. 7b, d, e). Moreover, these sources had obviously different seasonal
327 variation characteristics (Fig. 6). Long-range transport of biomass burning, nitration
328 reaction, and coal combustion were much more intense in winter than in other seasons
329 (Fig. 6a, c, d). Spring, autumn, and winter saw the most long-range transport of mixed
330 sources, whereas later summer and early autumn had the least amount of it (Fig. 6b). In

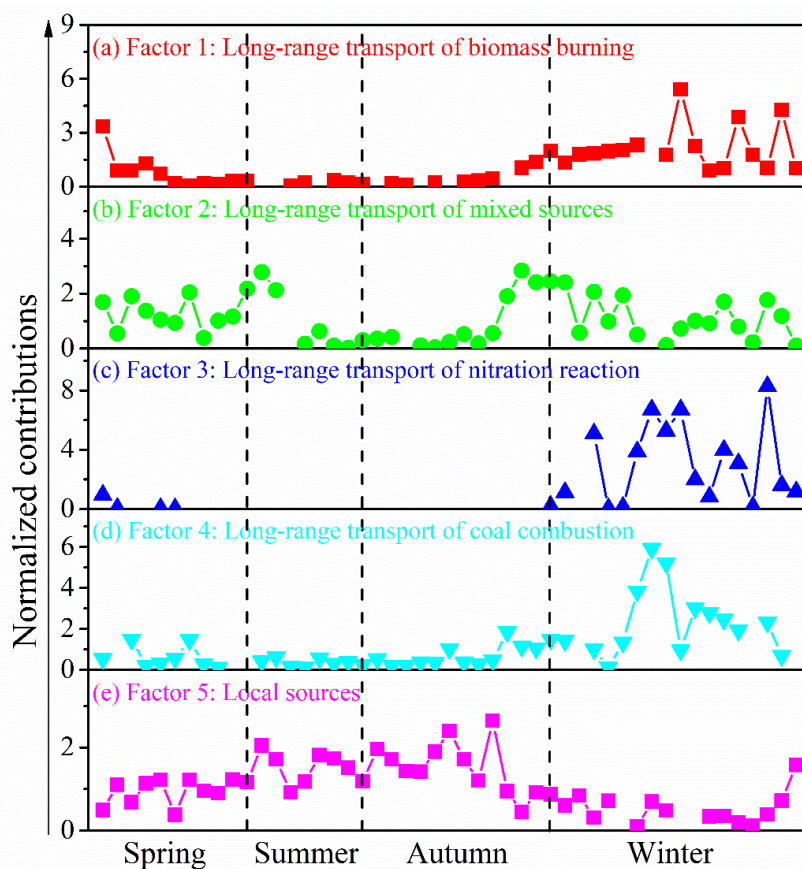


331 spring, summer, and autumn, contributions from local sources were higher than they
 332 were in winter (Fig. 6e).



333
 334
 335

Fig.5 Source profiles of NACs obtained from PMF analysis (ff *n*-alk.: ff *n*-alkane.
 lev.: levoglucosan. tre.: trehalose).



336
337
338

Fig. 6 Time variations of normalized contributions of each source.

339 During springtime, long-range transport of mixed sources had the biggest
340 influence on NACs, followed by the local sources, which accounted respectively for
341 37.1% and 31.3% of the total (Fig. 7b). For total NACs, the correlation coefficient
342 (Pearson r) was strong with SO_2 , ff-n-alkanes , PAHs , levoglucosan , and K^+ ($r > 0.73$,
343 $p < 0.01$), and the total NACs correlated well with NO_2 , O_3 , NO_3^- , and NH_4^+ ($r > 0.70$,
344 $p < 0.01$) (Table S2). The outcome indicated that NACs originate not only from primary
345 emissions but also from the secondary formation. Furthermore, The Pearson r for
346 levoglucosan ($r = 0.933$, $p < 0.01$) and NO_2 ($r = 0.945$, $p < 0.01$) were higher in comparison



347 to other parameters, suggesting that the burning of biomass and NO₂ had significant
348 effects on NACs at the summit of Mt. Wuyi in spring.

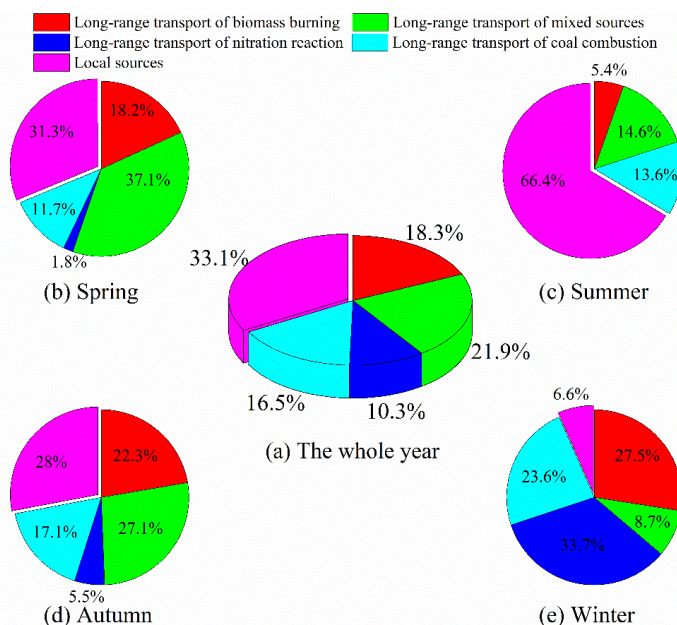
349 During summertime, local sources were the largest contributors to NACs, with the
350 relative contributions accounting for more than 65% of the total (Fig. 7c). The
351 correlation coefficient (Pearson *r*) of total NACs was strong with NO₂ ($r=0.869, p<0.01$),
352 O₃ ($r=0.786, p<0.01$), SO₄²⁻ ($r=0.884, p<0.01$), NO₃⁻ ($r=0.678, p<0.05$), and NH₄⁺
353 ($r=0.881, p<0.01$) (Table S3), further suggesting that the secondary formation
354 contributes significantly to the summertime NACs at the summit of Mt. Wuyi. The
355 secondary formation has been identified as a major cause of the origin of atmospheric
356 nitrated phenols, particularly in the summer, during the various field and modeling
357 investigations conducted recently (Yuan et al., 2016; Mayorga et al., 2021; Xie et al.,
358 2017; Cai et al., 2022; Wang et al., 2019). The strong associations between O₃ and
359 NACs further support the significance of photochemical oxidation for NACs. In
360 addition, Cai et al. discovered that in the summer metropolitan Shanghai, the majority
361 of NACs were enhanced via photo-oxidation (Cai et al., 2022).

362 During autumn, the relative contributions of each source of NACs were similar to
363 those observed in spring. Local sources and long-range transport of mixed sources made
364 almost equal contributions to NACs, which accounted for 28% and 27.1%, respectively
365 (Fig. 7d). Long-range transport of biomass burning also made a relatively large
366 contribution to NACs (22.3%). There was still a strong correlation between NACs and
367 NO₂ ($r=0.886, p<0.01$). It is noteworthy that the correlation coefficient (Pearson *r*) of
368 total NACs was stronger with SO₂ ($r=0.805, p<0.01$) and SO₄²⁻ ($r=0.615, p<0.05$), and



369 weaker with O₃ ($r=0.165$) in autumn than with the same in spring (Table S4). The
370 findings revealed that at the summit of Mt. Wuyi in autumn, the proportional
371 contribution of coal combustion was rising and the impact of photochemical reaction
372 was declining.

373 During wintertime, long-range transport of nitration reaction was the largest
374 contributor for NACs (33.7%), followed by long-range transport of biomass burning
375 (27.5%) and coal combustion (23.6%) (Fig. 7e). The total NACs correlated better with
376 NO₂ ($r=0.879$, $p<0.01$) than any other parameters (Table S5), thereby pointing towards
377 significant involvement of NO₂ in NACs formation. According to earlier research, coal
378 combustion and biomass burning had a greater contribution to NACs in the winter (Cai
379 et al., 2022), with direct emissions from biomass burning in the range of 0.4 to 11.1 mg
380 kg⁻¹ (Iinuma et al., 2007; Wang et al., 2017). Furthermore, earlier research suggested
381 that the detection of increased amounts of particulate phenols could be significantly
382 attributed to coal combustion activities. The emission factors ranged from 0.2 to 10.1
383 mg kg⁻¹ for bituminite, anthracite, lignite chunks, and briquettes. The residential coal
384 combustion resulted in a net emission of 178 ± 42 Mg of fine particles of nitrated
385 phenols, according to statistics of domestic coal consumption in a total of 30 provinces
386 in Chinese in 2016 (Lu et al., 2019b).



387

388

Fig. 7 Relative contributions of each source for NACs in different seasons.

389 3.4 Impact of NO₂ on NACs

390 Although NACs are highly affected by primary emissions, the secondary
391 formation was also a very important source of particulate NACs, and NO₂ was a very
392 important factor during the process (Ren et al., 2022; Cai et al., 2022). Studies have
393 revealed that there is a closer link between NACs and NO₂ for samples taken at night,
394 further pointing to the importance of NO₃[•]-initiated oxidation in the generation of
395 NACs at night (Wang et al., 2018; Li et al., 2020c; Cai et al., 2022). According to the
396 previous research, the intermediate formed when phenol reacts with either •OH during
397 in the daytime or NO₃[•] during the night produces phenoxy radical (C₆H₅O•), which is
398 where nitrophenol is produced (Berndt and Bge, 2003). The total measured NACs and
399 NO₂ in our study displayed comparable temporal fluctuations (Fig. 2e), and they

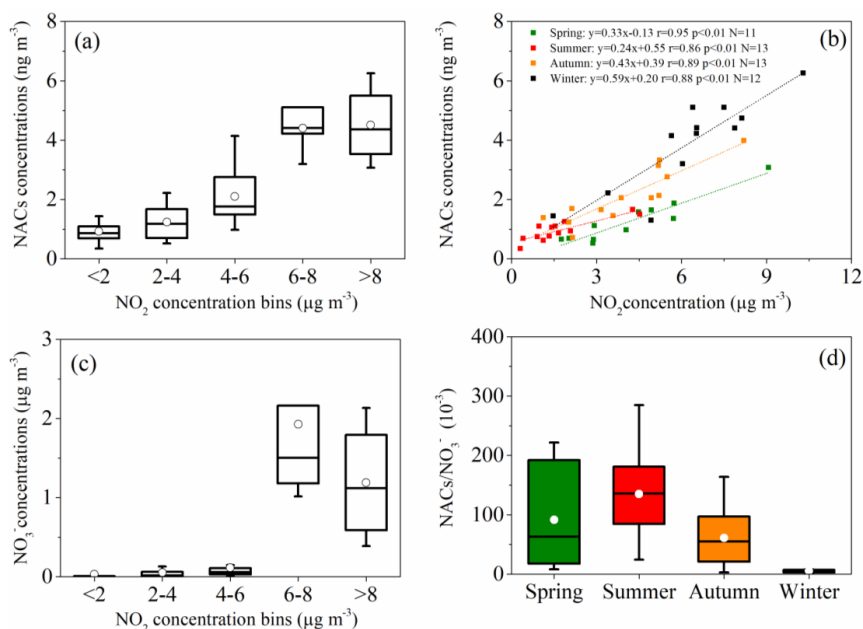


400 revealed strong correlations in the course of the entire campaign ($r=0.879$, $p<0.01$). The
401 concentrations of nitrate (NO_3^-) and total NACs as a function of NO_2 abundance, and
402 the fluctuations of $[\text{NACs}] / [\text{NO}_3^-]$ mass ratios were plotted in Fig. 8 to examine the
403 impact of NO_2 abundance further on the second generation of NACs and the current
404 form. According to earlier investigations, box whisker plots (Fig.6a, c) typically
405 showed higher NACs and NO_3^- concentrations with increasing NO_2 abundance (Cai et
406 al., 2022; Wang et al., 2018; Ren et al., 2022). Additionally, the encouraging effect of
407 NO_2 was more pronounced in winter than in other seasons (Fig. 8b), perhaps because
408 winter has much higher NO_x abundance with higher VOC precursor oxidation capacity
409 (Cai et al., 2022). Based on the results of SEM, the influence of the weight of NO_2 on
410 NACs was significantly greater than that of other factors in winter, such as *n*-alkane
411 and SO_2 , although they all had significant effects on NACs (Fig. 4b). Fig. 4d shows the
412 variations of $[\text{NACs}] / [\text{NO}_3^-]$ mass ratios during the whole campaign. This ratio was
413 much higher in comparison to that observed in urban sites (Cai et al., 2022; Wang et al.,
414 2018; Ren et al., 2022), would suggesting NACs were more likely generated in the
415 background site at low NO_x levels. According to certain studies conducted in urban
416 centers, when NO_2 levels were high ($\text{NO}_2>30\text{ppb}$), the NO_2 excess would be further
417 oxidized to generate inorganic nitrate, which would lead to a change in the relative
418 dominance of organic and inorganic compounds. When NO_2 was scarcer, a higher
419 portion of NO_2 was covered into organic nitrogen (Cai et al., 2022; Wang et al., 2018).
420 Here, the NO_2 levels on the summit of Mt. Wuyi were much lower than those in the
421 urban's atmosphere, with the ratio of $[\text{NACs}] / [\text{NO}_3^-]$ highest during summer than in



422 other seasons (Fig. 8d), all indicating that the formation of organic nitrated aerosols was
423 relatively sensitive to NO_2 at the low- NO_x level. Additionally, NO_2 may encourage the
424 synthesis of NACs and have a major impact on their composition, particularly for NCs
425 (Fig. 9a). When NO_2 levels were above 8 ppb, 4NP and 4NC both contributed more to
426 the total NACs, and the concentrations of NACs were at their maximum levels at those
427 levels (Fig. 9b).

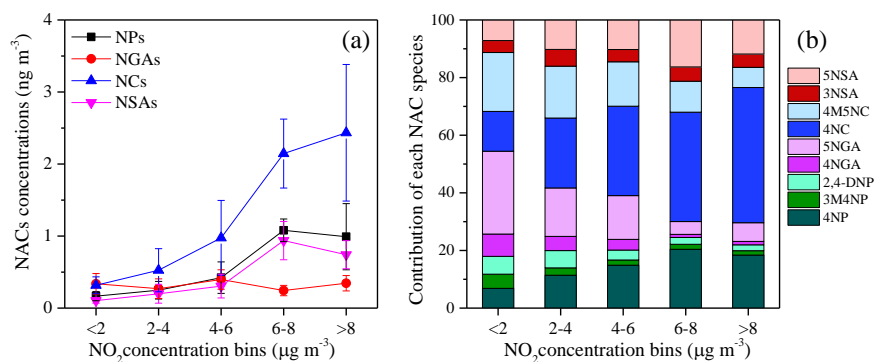
428



429

430 Fig. 8 Concentrations of NACs (a, b), nitrate (NO_3^-) (c) as a function of NO_2
431 concentration bins, and NACs / NO_3^- ratios (d) during the whole sampling time. The
432 mean values are represented by the markers and the 25th and 75th percentiles are
433 represented by whiskers.

434



435
436 Fig. 9 Concentrations of NACs (a) and (b) contribution of each NACs species as a
437 function of NO_2 concentration bins. (NPs: 4NP, 3M4NP, and 2,4-DNP; NGAs: 4NGA
438 and 5NGA; NCs: 4NC and 4M5NC; NSAs: 3NSA and 5NSA).

439

440 Different levels of NO_2 may have different effects on nitrate aerosols in different
441 atmospheric conditions, especially at high NO_x levels, although previous studies had
442 come to a consensus that organic nitrated aerosols were relatively sensitive to NO_2
443 under low levels. In Beijing, our prior research had shown that at NO_2 concentrations
444 above 30ppb, inorganic nitrates were converted more quickly during the day, while at
445 the night, there was a shift in the corresponding products of oxidation to predominantly
446 organic ones (Ren et al., 2022). The transition from organic- to inorganic-dominated
447 products takes place in line with the switch from low- to high- NO_x regimes according
448 to Wang et al., (2019), with low- NO_x conditions being predominated by organic-
449 dominated products and a switch from majorly organic-entities to inorganic ones at
450 high- NO_x conditions ($\text{NO}_2 \sim 25$ ppb for the night and $\text{NO}_2 \sim 20$ ppb for the day).
451 Inorganic nitrate predominated among the NO_x oxidation products in high- NO_x
452 concentrations ($\text{NO}_2 > 30$ ppb), according to Cai et al., (2022). These variations could be
453 caused by different precursor kinds and concentrations, as well as other variables.
454 Additional and more thorough research is required to fully understand the quantitative



455 impact of NO₂ on nitrate aerosols under various atmospheric conditions using
456 laboratory simulation and field measurements.

457 **4 Summary and conclusion**

458 NACs from samples of fine particle were examined at the peak of Mt. Wuyi in
459 2014 and 2015. Nine quantified NACs manifested a significant rise in overall
460 abundance in the winter and autumn, partly as a result of air masses traveling primarily
461 through northern heating regions. Over the year, 4-NC was the most prevalent species.
462 The majority of NACs were impacted by the primary emissions such as coal, biomass
463 and petroleum combustion. The transport of contaminants had a significant impact on
464 the atmospheric NACs at the peak of Mt. Wuyi, particularly in the winter and spring.
465 Under low-NO_x conditions, the production of organic nitrated aerosols was relatively
466 responsive to NO₂. For obtaining a more quantitative understanding of the influence of
467 NO₂ on nitrate aerosols under diverse atmospheric settings, additional thorough
468 examination through laboratory modeling and field measurements is required.

469

470 **Data availability**

471 The field observational and the lab experimental data used in this study are
472 available from the corresponding author upon request (Gehui Wang via
473 ghwang@geo.ecnu.edu.cn).



474 **Author contributions**

475 GW designed the research; JT and ZZ collected the samples; YR conducted the
476 experiments; YR and JW analyzed the data and wrote the paper; GW, JW and HL
477 contributed to the paper with useful scientific discussions and comments.

478 **Competing interests**

479 The authors declare that they have no conflict of interest.

480 **Acknowledgements**

481 This work is financially supported by the program from National Natural Science
482 Foundation of China (No. 41907197), the Fundamental Research Funds for Central
483 Public Welfare Scientific Research Institutes of China, Chinese Research Academy of
484 Environmental Sciences (No. 2019YSKY-018).

485

486

487 **References**

- 488 Berndt, T. and Bge, O.: Gas-phase reaction of OH radicals with phenol, PCCP, 5, 342-350,
489 <https://doi.org/10.1039/B208187C>, 2003.
- 490 Cai, D., Wang, X., George, C., Cheng, T., Herrmann, H., Li, X., and Chen, J.: Formation of
491 Secondary Nitroaromatic Compounds in Polluted Urban Environments, J. Geophys. Res.-
492 Atmos., <https://doi.org/10.1029/2021JD036167>, 2022.
- 493 Chen, H. Y. and Chen, L. D.: Importance of anthropogenic inputs and continental-derived dust
494 for the distribution and flux of water-soluble nitrogen and phosphorus species in aerosol



- 495 within the atmosphere over the East China Sea, *Journal of Geophysical Research*
496 *Atmospheres*, 113, D11303, <https://doi.org/10.1029/2007JD009491>, 2008.
- 497 Chen, Y. and Siefert, R. L.: Seasonal and spatial distributions and dry deposition fluxes of
498 atmospheric total and labile iron over the tropical and subtropical North Atlantic Ocean,
499 *Journal of Geophysical Research Atmospheres*, 109, D09305,
500 <https://doi.org/10.1029/2003JD003958>, 2004.
- 501 Chiapello, I., Bergametti, G., and Chaten, B.: Origins of African dust transported over the
502 northeastern tropical Atlantic, *Journal of Geophysical Research Atmospheres*, 102, 13701-
503 13709, <https://doi.org/10.1029/97JD00259>, 1997.
- 504 Chow, K. S., Huang, X. H. H., and Yu, J. Z.: Quantification of nitroaromatic compounds in
505 atmospheric fine particulate matter in Hong Kong over 3 years: field measurement evidence
506 for secondary formation derived from biomass burning emissions, *Environmental Chemistry*,
507 13, <https://doi.org/10.1071/EN15174>, 2015.
- 508 Comero, S., Capitani, L., and Gawlik, B.: Positive Matrix Factorisation (PMF)—An introduction
509 to the chemometric evaluation of environmental monitoring data using PMF, Office for
510 Official Publications of the European Communities, Luxembourg, 59, 2009.
- 511 Desyaterik, Y., Sun, Y., Shen, X., Lee, T., Wang, X., Tao, W., and Collett, J. L.: Speciation of
512 "brown" carbon in cloud water impacted by agricultural biomass burning in eastern China,
513 *Journal of Geophysical Research Atmospheres*, 118, 7389-7399,
514 <https://doi.org/10.1002/jgrd.50561>, 2013.
- 515 Finewax, Zachary, de, Gouw, Joost, A., Ziemann, Paul, and J.: Identification and Quantification
516 of 4-Nitrocatechol Formed from OH and NO₃ Radical-Initiated Reactions of Catechol in
517 Air in the Presence of NO_x: Implications for Secondary Organic Aerosol Formation from
518 Biomass Burning, *Environ. Sci. Technol.*, 52, 1981-1989,
519 <https://doi.org/10.1021/acs.est.7b05864>, 2018.
- 520 Harrison, M. A. J., Barra, S., Borghesi, D., Vione, D., Arsene, C., and Olariu, R. I.: Nitrated
521 phenols in the atmosphere: a review, *Atmos. Environ.*, 39, 231-248,
522 <https://doi.org/10.1016/j.atmosenv.2004.09.044>, 2005.
- 523 Iinuma, Y., Boge, O., Graefe, R., and Herrmann, H.: Methyl-Nitrocatechols: Atmospheric
524 Tracer Compounds for Biomass Burning Secondary Organic Aerosols, *Environ. Sci.*
525 *Technol.*, 44, 8453-8459, <https://doi.org/10.1021/es102938a>, 2010.
- 526 Iinuma, Y., Brüggemann, E., Gnauk, T., Müller, K., Andreae, M. O., Helas, G., Parmar, R., and
527 Herrmann, H.: Source characterization of biomass burning particles: The combustion of
528 selected European conifers, African hardwood, savanna grass, and German and Indonesian
529 peat, *J. Geophys. Res.-Atmos.*, 112, D08209, <https://doi.org/10.1029/2006JD007120>, 2007.
- 530 Kahnt, A., Behrouzi, S., Vermeylen, R., Shalamzari, M. S., Vercauteren, J., Roekens, E., Claeys,
531 M., and Maenhaut, W.: One-year study of nitro-organic compounds and their relation to
532 wood burning in PM₁₀ aerosol from a rural site in Belgium, *Atmos. Environ.*, 81, 561-568,
533 <https://doi.org/10.1016/j.atmosenv.2013.09.041>, 2013.
- 534 Kitanovski, Z., Grgic, I., Vermeylen, R., Claeys, M., and Maenhaut, W.: Liquid chromatography
535 tandem mass spectrometry method for characterization of monoaromatic nitro-compounds
536 in atmospheric particulate matter, *J. Chromatogr.*, 1268, 35-43,
537 <https://doi.org/10.1016/j.chroma.2012.10.021>, 2012.
- 538 Kitanovski, Z., Hovorka, J., Kuta, J., Leoni, C., Proke, R., Sáňka, O., Shahpoury, P., and



- 539 Lammel, G.: Nitrated monoaromatic hydrocarbons (nitrophenols, nitrocatechols,
540 nitrosalicylic acids) in ambient air: levels, mass size distributions and inhalation
541 bioaccessibility, *Environmental Science and Pollution Research*, 28, 59131–59140,
542 <https://doi.org/10.1007/S11356-020-09540-3>, 2021.
- 543 Li, J., Zhang, Q., Wang, G., Li, J., Wu, C., Liu, L., Wang, J., Jiang, W., Li, L., Ho, K. F., and
544 Cao, J.: Optical properties and molecular compositions of water-soluble and water-insoluble
545 brown carbon (BrC) aerosols in Northwest China, *Atmos. Chem. Phys.*, 20, 4889–4904,
546 <https://doi.org/10.5194/acp-20-4889-2020>, 2020a.
- 547 Li, M., Wang, X., Lu, C., Li, R., Zhang, J., Dong, S., Yang, L., Xue, L., Chen, J., and Wang, W.:
548 Nitrated phenols and the phenolic precursors in the atmosphere in urban Jinan, China, *Sci.*
549 *Total. Environ.*, 714, <https://doi.org/10.1016/j.scitotenv.2020.136760>, 2020b.
- 550 Li, X., Yang, Y., Liu, S., Zhao, Q., Wang, G., and Wang, Y.: Light absorption properties of
551 brown carbon (BrC) in autumn and winter in Beijing: Composition, formation and
552 contribution of nitrated aromatic compounds, *Atmos. Environ.*, 223,
553 <https://doi.org/10.1016/j.atmosenv.2020.117289>, 2020c.
- 554 Liang, Y., Wang, X., Dong, S., Liu, Z., Mu, J., Lu, C., Zhang, J., Li, M., Xue, L., and Wang, W.:
555 Size distributions of nitrated phenols in winter at a coastal site in north China and the impacts
556 from primary sources and secondary formation, *Chemosphere*, 250,
557 <https://doi.org/10.1016/j.chemosphere.2020.126256>, 2020.
- 558 Lin, P., Bluvshstein, N., Rudich, Y., Nizkorodov, S. A., Laskin, J., and Laskin, A.: Molecular
559 Chemistry of Atmospheric Brown Carbon Inferred from a Nationwide Biomass Burning
560 Event, *Environ. Sci. Technol.*, 51, 11561–11570, <https://doi.org/10.1021/acs.est.7b02276>,
561 2017.
- 562 Lu, C., Wang, X., Dong, S., Zhang, J., and Wang, W.: Emissions of fine particulate nitrated
563 phenols from various on-road vehicles in China, *Environ. Res.*, 179,
564 <https://doi.org/10.1016/j.envres.2019.108709>, 2019a.
- 565 Lu, C., Wang, X., Li, R., Gu, R., Zhang, Y., Li, W., Gao, R., Chen, B., Xue, L., and Wang, W.:
566 Emissions of fine particulate nitrated phenols from residential coal combustion in China,
567 *Atmos. Environ.*, 203, 10–17, <https://doi.org/10.1016/j.atmosenv.2019.01.047>, 2019b.
- 568 Lv, S., Wang, F., Wu, C., Chen, Y., Liu, S., Zhang, S., Li, D., Du, W., Zhang, F., Wang, H.,
569 Huang, C., Fu, Q., Duan, Y., and Wang, G.: Gas-to-aerosol phase partitioning of atmospheric
570 water-soluble organic compounds at a rural site of China: An enhancing effect of NH₃ on
571 SOA formation, *Environ. Sci. Technol.*, 56, 3915–3924,
572 <https://doi.org/10.1021/acs.est.1c06855>, 2022.
- 573 Mayorga, R. J., Zhao, Z., and Zhang, H.: Formation of secondary organic aerosol from nitrate
574 radical oxidation of phenolic VOCs: Implications for nitration mechanisms and brown
575 carbon formation, *Atmos. Environ.*, 244, <https://doi.org/10.1016/j.atmosenv.2020.117910>,
576 2021.
- 577 Mohr, C., Lopez-Hilfiker, F. D., Zotter, P., ħ, A. S. H. P., Xu, L., Ng, N. L., Herndon, S. C.,
578 Williams, L. R., Franklin, J. P., Zahniser, M. S., Worsnop, D. R., Knighton, W. B., Aiken, A.
579 C., Gorkowski, K. J., Dubey, M. K., Allan, J. D., and Thornton, J. A.: Contribution of
580 Nitrated Phenols to Wood Burning Brown Carbon Light Absorption in Detling, United
581 Kingdom during Winter Time, *Environ. Sci. Technol.*, 47, 6316–6324,
582 <https://doi.org/10.1021/es400683v>, 2013.



- 583 Ren, Y., Wei, J., Wang, G., Wu, Z., Ji, Y., and Li, H.: Evolution of aerosol chemistry in Beijing
584 under strong influence of anthropogenic pollutants: Composition, sources, and secondary
585 formation of fine particulate nitrated aromatic compounds, *Environ. Res.*, 204, 111982,
586 <https://doi.org/10.1016/j.envres.2021.111982>, 2022.
- 587 Ren, Y., Wang, G., Tao, J., Zhang, Z., Wu, C., Wang, J., Li, J., Wei, J., Li, H., and Meng, F.:
588 Seasonal characteristics of biogenic secondary organic aerosols at Mt. Wuyi in Southeastern
589 China: Influence of anthropogenic pollutants, *Environ. Pollut.*, 252, 493-500,
590 <https://doi.org/10.1016/j.envpol.2019.05.077>, 2019.
- 591 Teich, M., Van Pinxteren, D., Wang, M., Kecorius, S., Wang, Z., Müller, T., Mocnik, G., and
592 Herrmann, H.: Contributions of nitrated aromatic compounds to the light absorption of
593 water-soluble and particulate brown carbon in different atmospheric environments in
594 Germany and China, *Atmos. Chem. Phys.*, 17, 1653-1672, <https://doi.org/10.5194/acp-17-1653-2017>, 2017.
- 596 Wang, G., Zhou, B., Cheng, C., Cao, J., Li, J., Meng, J., Tao, J., Zhang, R., and Fu, P.: Impact
597 of Gobi desert dust on aerosol chemistry of Xi'an, inland China during spring 2009:
598 differences in composition and size distribution between the urban ground surface and the
599 mountain atmosphere, *Atmos. Chem. Phys.*, 13, 819-835, <https://doi.org/10.5194/acp-13-819-2013>, 2013.
- 601 Wang, G., Zhang, R., Gomez, M. E., Yang, L., Levy, Z. M., Hu, M., Lin, Y., Peng, J., Guo, S.,
602 and Meng, J.: Persistent sulfate formation from London Fog to Chinese haze, *Proc Natl Acad
603 Sci U S A*, 113, 13630-13635, <https://doi.org/10.1073/pnas.1616540113/-/DCSupplemental>
604 2016.
- 605 Wang, G., Cheng, C., Huang, Y., Tao, J., Ren, Y., Wu, F., Meng, J., Li, J., Cheng, Y., Cao, J.,
606 Liu, S., Zhang, T., Zhang, R., and Chen, Y.: Evolution of aerosol chemistry in Xi'an, inland
607 China, during the dust storm period of 2013 – Part I: Sources, chemical forms and formation
608 mechanisms of nitrate and sulfate, *Atmos. Chem. Phys.*, 14, 11571-11585,
609 <https://doi.org/10.5194/acp-14-11571-2014>, 2014.
- 610 Wang, L., Wang, X., Gu, R., Wang, H., Yao, L., Wen, L., Zhu, F., Wang, W., Xue, L., Yang, L.,
611 Lu, K., Chen, J., Wang, T., Zhang, Y., and Wang, W.: Observations of fine particulate nitrated
612 phenols in four sites in northern China: concentrations, source apportionment, and
613 secondary formation, *Atmos. Chem. Phys.*, 18, 4349-4359, <https://doi.org/10.5194/acp-18-4349-2018>, 2018.
- 615 Wang, X., Gu, R., Wang, L., Xu, W., Zhang, Y., Chen, B., Li, W., Xue, L., Chen, J., and Wang,
616 W.: Emissions of fine particulate nitrated phenols from the burning of five common types
617 of biomass, *Environ. Pollut.*, 230, 405-412, <http://dx.doi.org/10.1016/j.envpol.2017.06.072>,
618 2017.
- 619 Wang, Y., Hu, M., Wang, Y., Zheng, J., and Yu, J. Z.: The formation of nitro-aromatic
620 compounds under high NO_x and anthropogenic VOC conditions in urban Beijing, China,
621 *Atmos. Chem. Phys.*, 19, 7649-7665, <https://doi.org/10.5194/acp-19-7649-2019>, 2019.
- 622 Wu, C., Wang, G., Li, J., Li, J., Cao, C., Ge, S., Xie, Y., Chen, J., Li, X., Xue, G., Wang, X.,
623 Zhao, Z., and Cao, F.: The characteristics of atmospheric brown carbon in Xi'an, inland
624 China: sources, size distributions and optical properties, *Atmos. Chem. Phys.*, 20, 2017-
625 2030, <https://doi.org/10.5194/acp-20-2017-2020>, 2020.
- 626 Xie, M., Chen, X., Hays, M. D., Lewandowski, M., Offenberg, J. H., Kleindienst, T. E., and



- 627 Holder, A. L.: Light Absorption of Secondary Organic Aerosol: Composition and
628 Contribution of Nitroaromatic Compounds, *Environ. Sci. Technol.*, 51, 11607-11616,
629 <https://doi.org/10.1021/acs.est.7b03263>, 2017.
- 630 Yi Chen, Penggang Zheng, Zhe Wang, Wei Pu, Yan Tan, Chuan Yu, Men Xia, Weihao Wang,
631 Jia Guo, Dandan Huang, Chao Yan, Wei Nie, Zhenhao Ling, Qi Chen, Shuncheng Lee, and
632 Wang, T.: Secondary Formation and Impacts of Gaseous Nitro-Phenolic Compounds in the
633 Continental Outflow Observed at a Background Site in South China, *Environ. Sci. Technol.*,
634 56, 6933-6943, <https://doi.org/10.1021/acs.est.1c04596>, 2022.
- 635 Yuan, B., Liggio, J., Wentzell, J., Li, S. M., and Stark, H.: Secondary formation of nitrated
636 phenols: insights from observations during the Uintah Basin Winter Ozone Study (UBWOS)
637 2014, *Atmos. Chem. Phys.*, <https://doi.org/10.5194/acp-16-2139-2016>, 2016.
- 638 Zhang, X., Lin, Y. H., Surratt, J. D., and Weber, R. J.: Sources, Composition and Absorption
639 ngstrm Exponent of Light-absorbing Organic Components in Aerosol Extracts from the Los
640 Angeles Basin, *Environ. Sci. Technol.*, 47, 3685-3693, <https://doi.org/10.1021/es305047b>,
641 2013.
- 642 Zhang, Y. Y., Müller, L., Winterhalter, R., Moortgat, G. K., Hoffmann, T., and Poschl, U.:
643 Seasonal cycle and temperature dependence of pinene oxidation products, dicarboxylic
644 acids and nitrophenols in fine and coarse air particulate matter, *Atmos. Chem. Phys.*, 10,
645 7859-7873, <https://doi.org/10.5194/acp-10-7859-2010>, 2010.
- 646